SI to

Formation of highly-oxygenated organic molecules from α-pinene ozonolysis: chemical characteristics, mechanism and kinetic model development.

Ugo Molteni[1], Mario Simon[2], Martin Heinritzi[2], Christopher R. Hoyle[1,a], Anne-Kathrin Bernhammer[3], Federico Bianchi[4], Martin Breitenlechner[5,b], Sophia Brilke[2,c], António Dias[6], Jonathan Duplissy[4,11], Carla Frege[1], Hamish Gordon[7], Claudia Heyn [1], Tuija Jokinen[4], Andreas Kürten[2], Katrianne Lehtipalo[4,8], Vladimir Makhmutov[9], Tuukka Petäjä[4], Simone M. Pieber[10,d], Arnaud P. Praplan[8], Siegfried Schobesberger[4,12], Gerhard Steiner[5], Yuri Stozhkov[9], António Tomé[13], Jasmin Tröstl[1], Andrea C. Wagner[2], Robert Wagner[4], Christina Williamson[2,e,f], Chao Yan[4], Urs Baltensperger[1], Joachim Curtius[2], Neil M. Donahue[14], Armin Hansel[3,5], Jasper Kirkby[2,15], Markku Kulmala[4,11,16], Douglas R. Worsnop[4,17] and Josef Dommen[1,*].

*Corresponding Author: Dommen, Josef; e-mail: josef.dommen@psi.ch

[1] Laboratory of Atmospheric Chemistry, Paul Scherrer Institute, CH-5232 Villigen

[2] Institute for Atmospheric and Environmental Sciences, Goethe University Frankfurt, 60438 Frankfurt am Main, Germany

[3] Ionicon GesmbH, Innsbruck, Austria

[4] Institute for Atmospheric and Earth System Research INAR/Physics, Faculty of Science, University of Helsinki, P.O. Box 64, FI-00014 Helsinki, Finland

[5] Institute for Ion and Applied Physics, University of Innsbruck, 6020 Innsbruck, Austria

[6] Faculty of Sciences, University of Lisbon, Campo Grande 016, 1749-016 Lisboa, Portugal

[7] University of Leeds, LS2 9JT, United Kingdom

[8] Finnish Meteorological Institute, Erik Palménin aukio 1, 00560 Helsinki, Finland

[9] Lebedev Physical Institute of the Russian Academy of Sciences, 119991, Moscow, Leninsky prospekt, 53, Russia

[10] Department of Environmental Systems Science, ETH Zurich, Zurich, Switzerland

[11] Helsinki Institute of Physics, FI-00014 Helsinki, Finland

[12] University of Eastern Finland, Department of Applied Physics, P.O. Box 1627, 70211 Kuopio, Finland

[13] IDL-Universidade da Beira Interior, Covilhã, Portugal

[14] Center for Atmospheric Particle Studies, Carnegie Mellon University, Pittsburgh, PA 15213

[15] CERN, CH-1211 Geneva, Switzerland

[16] Aerosol and Haze Laboratory, Beijing University of Chemical Technology, Beijing, China

[17] Aerodyne Research Inc., 45 Manning Road, Billerica, MA 01821, USA

Present affiliations:

[a]Institute for Atmospheric and Climate Science, ETH Zurich, 8092 Zurich, Switzerland

[b]John A. Paulson School of Engineering and Applied Sciences, Harvard University, Cambridge, MA 02138, USA

[c]Faculty of Physics, University of Vienna, 1090 Vienna, Austria
[d]Laboratory for Air Pollution and Environmental Technology (Empa), CH-8600 Duebendorf, Switzerland
[e]Cooperative Institute for Research in Environmental Sciences, University of Colorado, Boulder, 80309, U.S.A
[f]NOAA Earth System Research Laboratory, Boulder, 80305, U.S.A

The supplementary information includes:

Description of: the experimental set up, mass spectrometer and list of experiments (Table S1). Information on the development of the MCM kinetic model add-on, evaluation of the HOM collision rate and the derivation of reaction rate constants (Table S2, S3, S4). Graphical Presentations of the autoxidation schemes (Scheme S1, S2, S3) and radical fragmentation (Scheme 4, 5). Simulated RO_2 and HO_2 concentrations (Figure S1).

Experimental SI. The CLOUD chamber is a 3 m diameter, 26.1 m^3 volume electro polished stainless-steel continuously stirred-tank reactor. In order to ensure highest cleanliness standards before starting the experiments, we follow a cleaning protocol, which consists of rinsing the chamber walls with ultra-clean water, and thereafter increasing the temperature up to 373 K and exposing the chamber to few ppmv of O_3 while continuously flushing it with clean air. Synthetic air is produced by evaporation of cryogenic nitrogen and oxygen, and humidification is done using ultra-clean water (Millipore Super-Q filters). α-Pinene (Sigma Aldrich 99%) was injected from a temperature-controlled evaporator using N_2 as a carrier gas. Furthermore, the chamber is always operated with 5 mbar overpressure. The combination of these measures ensures extremely low levels of contamination with organic vapours in the sub-pptv level.[1] Further information regarding the CLOUD chamber and instrumentation is available from our previous publications.[1,2]

Gas phase HOM from AP ozonolysis were detected with a nitrate chemical ionization mass spectrometer (nitrate-CIMS).[3,4] The instrument was initially developed to detect gas phase sulphuric acid and turned out to be very selective for HOM detection.[5] Nitric acid vapour is ionized by a corona discharge and nitrate ions are then mixed due to an electrostatic field with the sample flow from the CLOUD chamber. Analyte detection occurs via the following reactions;

$$A + NO_3^-\cdot(HNO_3)_n \rightarrow A\cdot NO_3^- + nHNO_3 \quad \textbf{RS 1}$$

$$A + NO_3^-\cdot(HNO_3)_n \rightarrow A^- + (n+1)HNO_3 \quad \textbf{RS 2}$$

where *n* in the nitrate-nitric acid anion clusters can vary from 0 to 2. The analyte (A) can be detected as an adduct with the nitrate ion (RS 1) or as a deprotonated anion (RS 2). The formed ions are transferred to a time-of-flight mass analyser (ToF) via 2 quadrupoles and an ion lens set. In the atmospheric pressure interface the air pressure is gradually reduced using a scroll pump and a 3-stage turbo molecular pump[6] from the inlet ambient pressure to the ToF section (~ 10^{-6} mbar).

In one experiment (run 1212.02) nitric acid was replaced with isotopically labeled ^{15}N nitric acid. For convenience all ions are reported here without the isotope label.

Master Chemical Mechanism HOM add-on, SI. The model was run with the conditions of the CLOUD chamber, i.e. a dilution rate of $1\cdot10^{-4}$ s^{-1} and typical wall loss rates for HOM species of $1.1\cdot10^{-3}$ s^{-1}.[1] AP and ozone

were constrained to the measured values. The condensational sink of HOM to aerosol is thought to become important only at very high AP_{react} and extended duration of the experiment, when particles grow to sufficient size to provide a substantial sink; its implementation is therefore outside the scope of this work. Therefore, the condensation sink of HOM to the particles is not included in the simulation. We tuned the reaction rate constants in a heuristic way to achieve good agreement with the experimental data. A more objective fine tuning of the rate constants could be achieved with algorithmic methods, but is beyond the work presented here.

HOM collision rate SI. The HOM collisional rate was calculated for the radicals $C_{10}H_{15}O_{5\text{-}10}$. The structures of the 6 HOM radicals were selected as suggested by Kirkby et al.[1]. They were optimized with Avogadro[7] by using MMF94. Collisional cross sections were obtained by using the software Sigma[8]. Values span between 95.1 and 106.3 $Å^2$, which correspond to a collision rate between 9.0 10^{-10} and 8.5 10^{-10} cm^3 $molecule^{-1}$ s^{-1}.

RO_2 reactions. The reaction rate constant for reaction R4a from the graphs in Figure.5 were derived as following:

The three pathways to $C_{10}H_{14}O_x$ are either via unimolecular decomposition of the peroxy radical (R2) or via reaction of the $C_{10}H_{15}O_x$ radicals with any other RO_2 either by reaction (R4a) or the alkoxy channel (R5). The rate determining step of the alkoxy channel is the alkoxy formation (R4b) which is followed by reaction R5 to the carbonyl compound as well as isomerization or decomposition (R6). For large and highly oxygenated compounds the latter two channels dominate and only a minor fraction α will take reaction path R5.

$$\frac{d[C_{10}H_{14}O_{odd}]}{dt} = k_{4a}[C_{10}H_{15}O_{even}][RO_2] + \alpha k_{4b}[C_{10}H_{15}O_{even}] + k_2[C_{10}H_{15}O_{even}] - k_w[C_{10}H_{14}O_{odd}] \qquad \text{(E1)}$$

At steady state the concentration of $C_{10}H_{15}O_{even}$ becomes:

$$[C_{10}H_{14}O_{odd}] = \frac{(k_4+\propto k_{4b})[C_{10}H_{15}O_{even}][RO_2]+k_2[C_{10}H_{15}O_{even}]}{k_w} \qquad \text{(E2)}$$

Dividing the equation by $C_{10}H_{15}O_{even}$ yields:

$$\frac{[C_{10}H_{14}O_{odd}]}{[C_{10}H_{15}O_{even}]} = \frac{(k_{4a}+\propto k_{4b})}{k_w}[RO_2]+\frac{k_2}{k_w} \quad \text{(E3)}$$

For small values of α we can approximate:

$$\frac{[C_{10}H_{14}O_{odd}]}{[C_{10}H_{15}O_{even}]} = \frac{(k_{4a})}{k_w}[RO_2]+\frac{k_2}{k_w} \qquad \text{(E4)}$$

Equation E4 is assumed for Figure 5a and a similar derivation can be applied for Figure 5b.

$C_{10}H_{16}O_{odd}$ is formed by the reaction of $C_{10}H_{15}O_{even}$ with RO_2 (R4a) or of $C_{10}H_{15}O_{odd}$ with HO_2 (R3a). The reaction rate constant of HO_2 with RO_2 is about $2.5.10^{-11}$ cm^3 s^{-1} and thus up to two orders of magnitude faster than RO_2 - RO_2 reactions. On the other hand $C_{10}H_{15}O_{even}$ concentrations are about a factor of 10 higher and the RO_2:HO_2 ratio is in the range of 100 – 1000. Thus, overall reaction R3a should yield a minor contribution to $C_{10}H_{16}O_{odd}$. Therefore, its formation rate can be written as:

$$\frac{d[C_{10}H_{16}O_{odd}]}{dt} = k_{4a}[C_{10}H_{15}O_{even}][RO_2] - k_w[[C_{10}H_{16}O_{odd}] \qquad \text{(E5)}$$

At steady state we obtain:

$$\frac{[C_{10}H_{16}O_{odd}]}{[C_{10}H_{15}O_{even}]} = \frac{k_{4a}[RO_2]}{k_w} \qquad \text{(E6)}$$

References SI.

(1) Kirkby, J.; Duplissy, J.; Sengupta, K.; Frege, C.; Gordon, H.; Williamson, C.; Heinritzi, M.; Simon, M.; Yan, C.;

Almeida, J.; et al. Ion-Induced Nucleation of Pure Biogenic Particles. *Nature* **2016**, *533* (7604), 521–526.

(2) Kirkby, J.; Curtius, J.; Almeida, J.; Dunne, E.; Duplissy, J.; Ehrhart, S.; Franchin, A.; Gagné, S.; Ickes, L.; Kürten, A.; et al. Role of Sulphuric Acid, Ammonia and Galactic Cosmic Rays in Atmospheric Aerosol Nucleation. *Nature* **2011**, *476* (7361), 429–433.

(3) Kürten, a.; Rondo, L.; Ehrhart, S.; Curtius, J. Performance of a Corona Ion Source for Measurement of Sulfuric Acid by Chemical Ionization Mass Spectrometry. *Atmos. Meas. Tech.* **2011**, *4* (3), 437–443.

(4) Jokinen, T.; Sipilä, M.; Junninen, H.; Ehn, M.; Lönn, G.; Hakala, J.; Petäjä, T.; Mauldin, R. L.; Kulmala, M.; Worsnop, D. R. Atmospheric Sulphuric Acid and Neutral Cluster Measurements Using CI-APi-TOF. *Atmos. Chem. Phys.* **2012**, *12* (9), 4117–4125.

(5) Ehn, M.; Thornton, J. a.; Kleist, E.; Sipilä, M.; Junninen, H.; Pullinen, I.; Springer, M.; Rubach, F.; Tillmann, R.; Lee, B.; et al. A Large Source of Low-Volatility Secondary Organic Aerosol. *Nature* **2014**, *506* (7489), 476–479.

(6) Junninen, H.; Ehn, M.; Petäjä, T.; Luosujärvi, L.; Kotiaho, T.; Kostiainen, R.; Rohner, U.; Gonin, M.; Fuhrer, K.; Kulmala, M.; et al. A High-Resolution Mass Spectrometer to Measure Atmospheric Ion Composition. *Atmos. Meas. Tech.* **2010**, *3* (4), 1039–1053.

(7) Hanwell, M. D.; Curtis, D. E.; Lonie, D. C.; Vandermeerschd, T.; Zurek, E.; Hutchison, G. R. Avogadro: An Advanced Semantic Chemical Editor, Visualization, and Analysis Platform. *J. Cheminform.* **2012**, *4* (8), 1–17.

(8) Wyttenbach, T.; Helden, G.; Batka, J. J.; Carlat, D.; Bowers, M. T. Effect of the Long-Range Potential on Ion Mobility Measurements. *J. Am. Soc. Mass Spectrom.* **1997**, *8* (3), 275–282.

(9) MathWorks. MATLAB. 2016.

(10) Kurtén, T.; Rissanen, M. P.; Mackeprang, K.; Thornton, J. A.; Hyttinen, N.; Jørgensen, S.; Ehn, M.; Kjaergaard, H. G. Computational Study of Hydrogen Shifts and Ring-Opening Mechanisms in α-Pinene Ozonolysis Products. *J. Phys. Chem. A* **2015**, *119* (46), 11366–11375.

Table S1. **CLOUD 8 experiments used in the present work.** Experiment label, ion condition N (neutral) or GCR (galactic cosmic ray) and AP concentration are reported.

Run Number	Condition	[AP] (ppt)
1208.03	N	22
1208.04	GCR	17
1208.07	N	51
1208.08	GCR	45
1208.10	N	108
1209.01	N	237
1209.02	GCR	226
1210.02	N	265
1210.04	GCR	526
1212.02	N	1692

Table S2. **$C_{20}H_{30}O_x$ dimers formed from RO_2-RO_2' recombination.** The numbers give the number of oxygen atoms (x) in the dimers. In blue dimers with an even oxygen number, in green dimers with an odd oxygen number.

	RO_2'					
RO_2	**Oxygen number**	**8**	**9**	**10**	**11**	**12**
	5				14	15
	6			14	15	16
	7		14	15	16	17
	8	14	15	16	17	18
	9		16	17	18	
	10			18		

Table S3: **Reaction rate constants *k* for dimer formation.** Rate constants were calculated with a nonnegative linear least squares analysis (Isqnonneg from MATLAB, Ref.[9]). Column 2 gives the RO_2-RO_2' recombination from Table S2. Column 3 gives the fitted values using all variables in Eq. (2) and (3). Column 3 uses only the main contributing RO_2-RO_2' recombination.

Dimer	combination	k (all reactions)	k (reduced reactions)
$C_{20}H_{30}O_{14}$	O5_O11	1.04E-07	removed
	O6_O10	**0**	0
	O7_O9	1.47E-09	removed
	O8_O8	2.61E-10	3.16E-10
$C_{20}H_{30}O_{15}$	O12_O5	1.06E-08	removed
	O11_O6	**0**	removed
	O10_O7	9.26E-10	8.69E-10
	O9_O8	5.84E-10	6.61E-10
$C_{20}H_{30}O_{16}$	O12_O6	9.82E-09	removed
	O11_O7	3.46E-08	removed
	O10_O8	1.80E-10	2.26E-10
	O9_O9	**0**	removed
$C_{20}H_{30}O_{17}$	O12_O7	**0**	removed
	O11_O8	5.37E-10	4.44E-10
	O10_O9	2.15E-10	1.78E-10
$C_{20}H_{30}O_{18}$	O12_O8	3.49E-10	1.60E-10
	O11_O9	2.28E-08	removed
	O10_O10	6.93E-11	8.18E-11

Table S4: **Reaction rate constants *k* for H-shift reactions in the MCM add-on.**

$C_{10}H_{15}O_4$ → $C_{10}H_{15}O_6$	k (s^{-1})
C107O2 → C107O2O2	$0.75\ 10^{-3}$
C109O2 → C107O2O2	$1.50\ 10^{-3}$
C10BO2 → C107O2O2	$1.50\ 10^{-3}$
$C_{10}H_{15}O_6$ → $C_{10}H_{15}O_8$	
C107O2O2 → C107O4O2	$2.40\ 10^{-1}$
$C_{10}H_{15}O_8$ → $C_{10}H_{15}O_{10}$	
C107O4O2 → C107O6O2	$2.20\ 10^{-1}$
$C_{10}H_{15}O_{10}$ → SINK	
C107O6O2 → SINK	$1.30\ 10^{-1}$

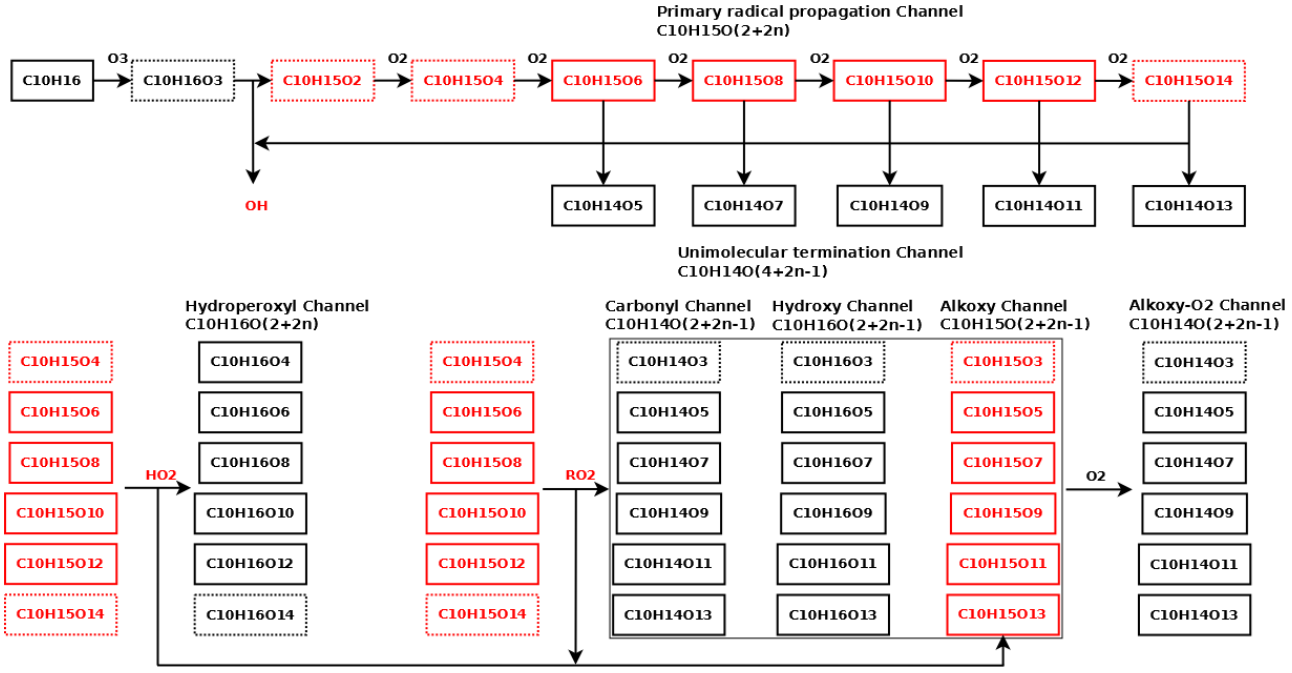

Scheme S1. **α-Pinene ozonolysis autoxidation radical propagation and first-generation products (n ≥ 1, number of oxygen molecules taken up after the vinoxy radical).** Radical species are presented in red font, closed shell compounds are presented in black font. Dashed frames indicate species that were not detected during the experiments.

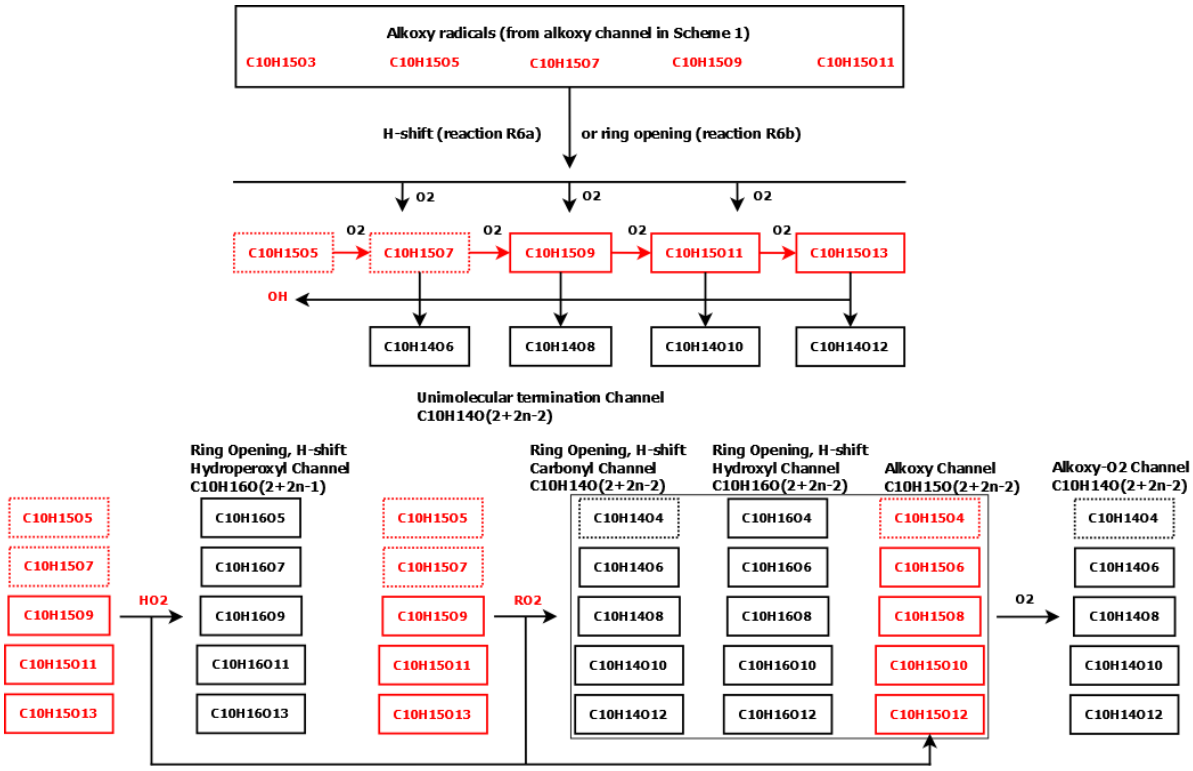

Scheme S2. **α-Pinene ozonolysis autoxidation radical propagation after the formation of alkoxy radicals (alkoxy channel in Scheme 1) and second-generation products (n > 1).** Radical species are presented in red font, closed shell compounds are presented in black font. Dashed frames indicate species that were not detected during the experiments.

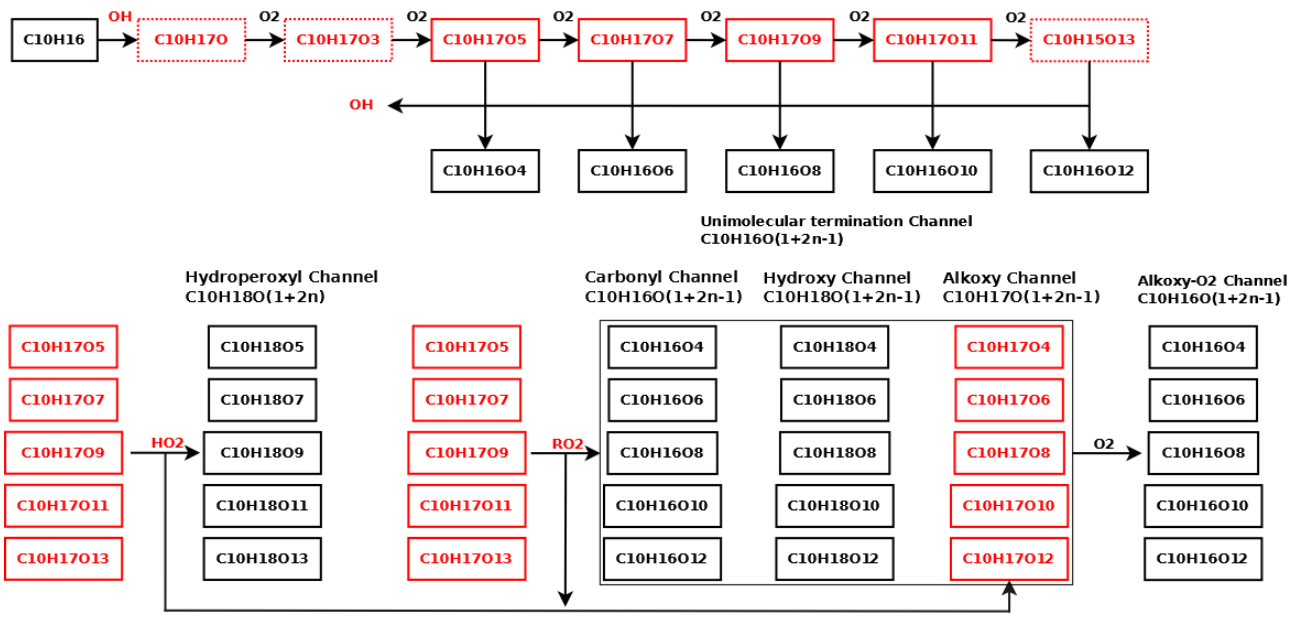

Scheme S3. ***α*-Pinene OH radical autoxidation radical propagation and first-generation products (n ≥ 2).** Radical species are presented in red font, closed shell compounds are presented in black font. Dashed frames indicate species that were not detected during the experiments.

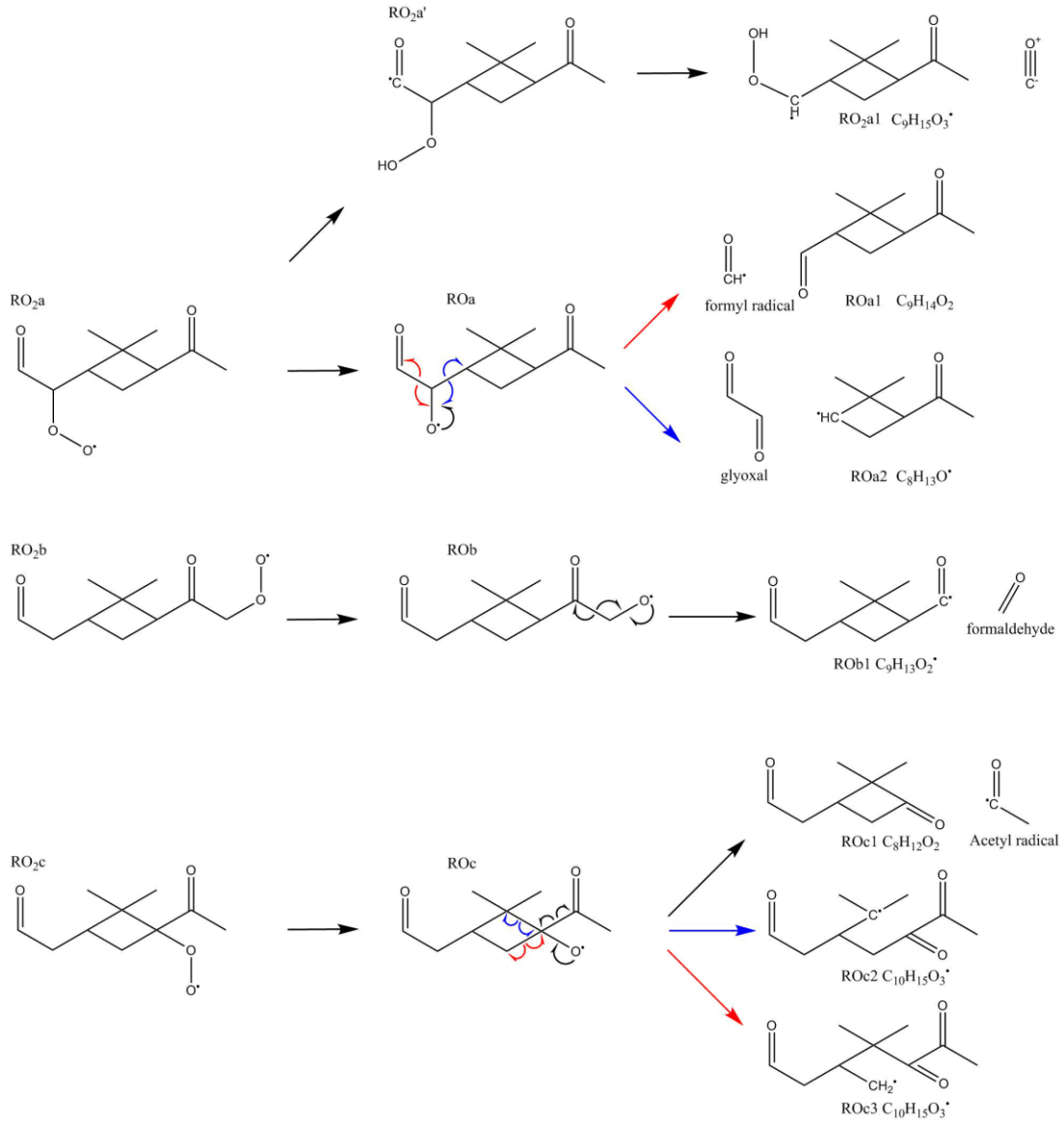

Scheme S4. **Alkoxy radical formation and bond recombination starting from the structures suggested by Kurtén et al. (2015)[10].** Coloured arrows help in separating different fragmentation ways. When the carbon backbone is not retained the fragmentation leads to a closed-shell molecule and a radical. Depending on the mechanism the un-paired electron resides on the large fraction of the parent radical or on a small (C1-2) carbon fragment.

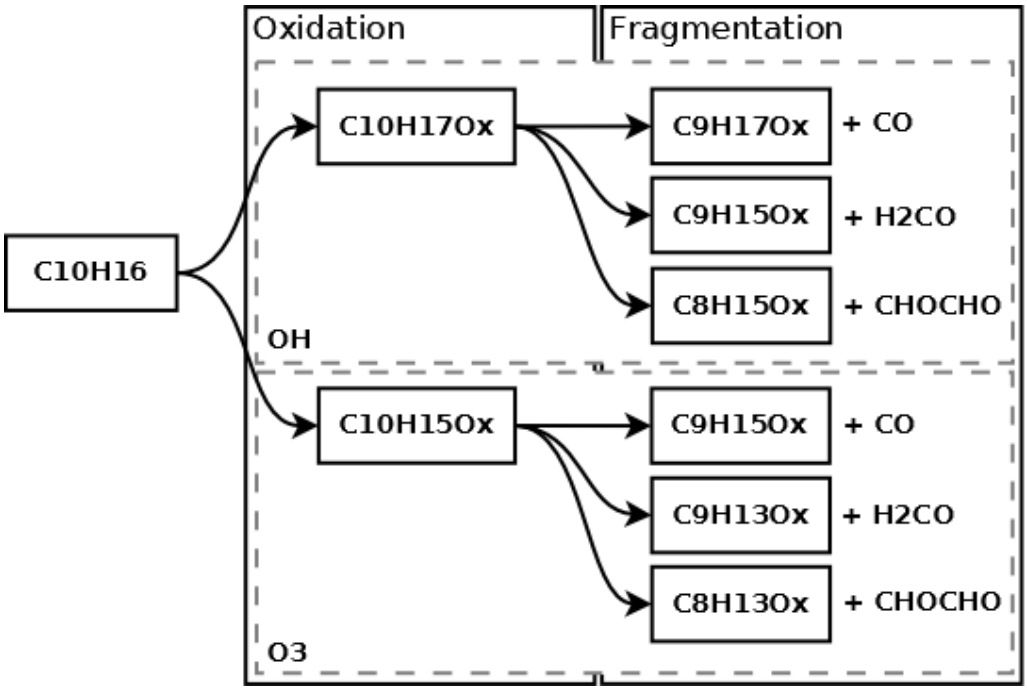

Scheme S5. Peroxy radical species ($C_{10}H_{17}O_x$ and $C_{10}H_{15}O_x$) from α-pinene OH radical and ozonolysis autoxidation, and corresponding peroxy radical species resulting from a further fragmentation step ($C_9H_{17}O_x$, $C_9H_{15}O_x$, $C_8H_{15}O_x$ and $C_9H_{15}O_x$, $C_9H_{13}O_x$, $C_8H_{13}O_x$).

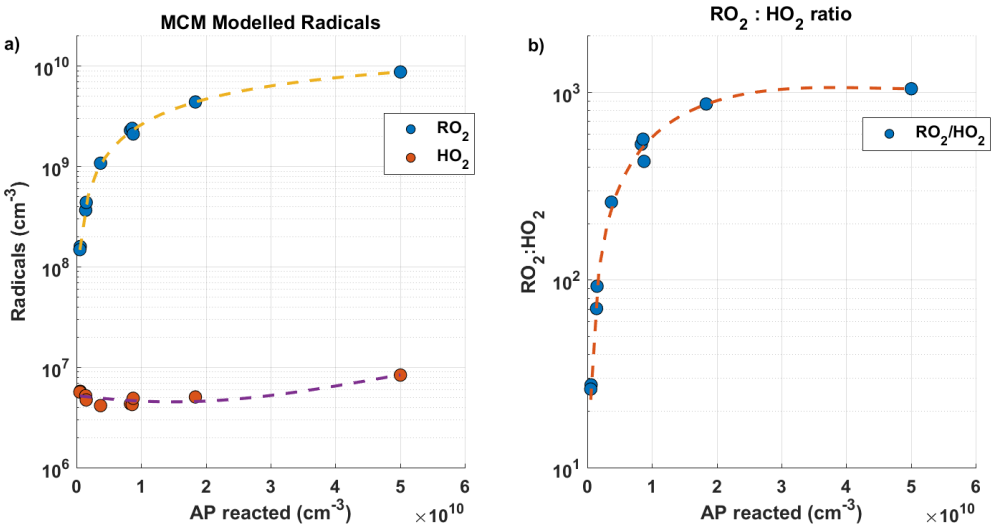

Figure S1. **RO_2 and HO_2 concentrations modeled with MCM. a)** RO_2 (blue) and HO_2 (orange) concentrations as a function of the reacted AP. RO_2 concentrations are fitted with a 3rd order polynomial equation (yellow line), HO_2 concentrations are fitted with a 2nd order polynomial equation (purple line). **b)** RO_2:HO_2 ratio as a function of the AP reacted. A 3rd order polynomial fit (orange) is added to guide the eye.